

1 **Documentation of the Conceptual Design of a Compact Photon**
2 **Source (CPS)**

3 E. Chudakov,¹ D. Day,² P. Degtiarenko,¹ R. Ent,¹ D.J. Hamilton,³
4 T. Horn,^{4,1,*} D. Keller,² C. Keppel,¹ G. Niculescu,⁵
5 P. Reid,⁶ I. Strakovsky,⁷ B. Wojtsekhowski,¹ and J. Zhang²

6 ¹*Jefferson Lab*

7 ²*University of Virginia*

8 ³*University of Glasgow*

9 ⁴*Catholic University of America*

10 ⁵*James Madison University*

11 ⁶*Saint Mary's University*

12 ⁷*George Washington University*

* Contact email: hornt@cua.edu

I Executive Summary

This document describes the technical design concept of a compact, high intensity photon source (CPS) producing 10^{12} equivalent photons per second with large gain in figure-of-merit (factor of ~ 30) to be used with dynamically nuclear polarized targets to measure processes such as Wide-Angle and Timelike Compton Scattering (WACS and TCS). Compared to the traditional bremsstrahlung photon source, the proposed solution will present several advantages, including much lower radiation levels, both prompt and post-operational due to the beam line elements radio-activation. For use with polarized targets, the heat load and radiation damage effects are well within the acceptable range. The design is flexible allowing the CPS to be converted into a K_L beam for spectroscopy experiments. PAC43-PAC45 at Jefferson Lab have seen several proposals and LOIs that require the CPS. One of these is C12-17-008 (Polarization Observables in Wide-Angle Compton Scattering at large s , t , and u), which was conditionally approved w/ Technical Review. The issues stated in the PAC45 report to be addressed are: 1) Finalize the design and price estimate for CPS, 2) Clearly establish the expected maximum photon intensity. **The goal of this document is to address the PAC45 technical comments for full approval of C12-17-008.**

The CPS design features a magnet, a central copper absorber, and hermetic shielding consisting of tungsten powder and borated plastic. The addition of the latter has considerable impact on reducing the neutron flux. The logic behind this design is that radiation from the source should be a few times less than from a photon beam interacting with the material of a polarized target. The equivalent heat load for a pure photon beam impinging such targets corresponds to a photon flux originating from a $2.7 \mu\text{A}$ electron beam current striking a 10% Cu radiator. Detailed simulations of the power density and heat flow analysis show that the maximum temperature in the absorber is below 400 degrees, well in the acceptable range of copper, and thus demonstrating that the CPS can absorb 30 kW in total (corresponding to 11 GeV beam energy and $2.7 \mu\text{A}$ beam current). Cooling of the core requires about four gallons of water per minute at a pressure of 110 psi (at 30 degree temperature rise).

The CPS fulfills the requirements on operational dose rates at JLab. This was established with extensive and realistic simulations. The projected prompt dose rate at the site boundary is less than $1 \mu\text{rem/hr}$ ($2.4 \mu\text{rem/hr}$ corresponds to a typical experiment at Jefferson Lab not requiring extra shielding). The activation dose outside the device envelope at one foot distance is less than several mrem/h after one hour following the end of a 1000 hour run (~ 40 PAC days). The activation dose at the pivot in the experimental target area, where operational maintenance tasks may be required, is dominated by the dose induced by a pure photon beam, and at one foot distance from the scattering chamber it is less than several mrem/h after one hour following the end of a 1000 hour run. i.e., the additional dose induced by radiation of the main beam absorbed in the Compact Photon Source is negligible.

In summary, the CPS shielding design provides a photon flux of 10^{12} equivalent photons/s, at a factor of 1000 reduction in prompt radiation dose compared to a $2.7 \mu\text{A}$ (30 kW) electron beam current striking a 10% Cu radiator, and is thus optimized to meet the acceptable radiation level requirements for a typical run time of 1000 hours, and with the photon source as close to the target as possible. The technical design and

58 installation in the existing hall infrastructure is feasible. The estimated cost is on the
59 order of \$2M and dominated by the cost of tungsten.

60 This document is organized as follows. In section II, we outline the science gain
61 with CPS in combination with dynamically nuclear polarized targets including the use
62 of an effective rastering of the beam at these high intensities. The heat load and power
63 deposition are also discussed. In section III, the conceptual design and components of
64 the CPS are discussed. Section IV lists the requirements a CPS has to meet to fulfill op-
65 erational dose rates at Jefferson Lab. In section V, we discuss the results of our shielding
66 design and optimization studies and compare them with the requirements in section IV.
67 Section VI deals with safety and engineering aspects including assembly/disassembly of
68 the CPS and a preliminary cost analysis. Appendix 1 describes the CPS concept transfer
69 to Hall D. Appendix 2 includes a benchmark comparison of the different simulations used
70 in our shielding design studies.

71 II Motivation: Science Gain with CPS

72 A Polarization Observables in Wide-Angle Compton 73 Scattering

74 The three-dimensional nucleon structure has been an active field, especially during
75 the last two decades since the invention of GPD formalism, and continues to be central
76 to the hadron physics at JLab. GPD formalism provides a unified description of such
77 important reactions as elastic electron scattering, DIS, DVCS/TCS, WACS and several
78 meson production channels. They are all described by a single set of four functions
79 E, H and \tilde{E}, \tilde{H} . These functions need to be modeled with parameters which should be
80 determined from the experimental data.

81 The WACS experimental observables provide several constraints for GPDs which
82 are complementary to other exclusive reactions due to an e_a^2 factor and an additional
83 $1/x$ weighing in the GPD integrals for WACS, e.g. the elastic form factor $F_1(t) =$
84 $\sum_a e_a \int dx H^a(x, 0, t)$ in contrast to the WACS vector form factor $R_V(t) = \sum_a e_a^2$
85 $\int \frac{dx}{x} H^a(x, 0, t)$, both of which are based on the same GPD $H(x, 0, t)$. In addition, for the
86 $\tilde{H}(x, \xi, t)$ the WACS axial form factor $R_A(t)$ provides much more accurate data than an
87 alternative constraint from the nucleon axial form factor.

88 The experiment needs to be performed at large photon energy and scattering angle
89 where the GPD-based calculations have good and predictable accuracy ($s, |t|, |u| > 2.5 \text{ GeV}^2$).
90 The experimental challenges associated with double-polarization measurements of photon-
91 induced reactions at high momentum transfer are formidable. Detector rate capabilities
92 and radiation hardness are both severely tested in beam-recoil measurements as a result
93 of a rapid decrease in recoil proton polarimeter analyzing power at high $-t$. Utilization
94 of a mixed electron-photon bremsstrahlung beam, on the other hand, limits luminosity
95 in beam-target measurements due to loss of target polarization, primarily as a result of
96 electron-induced heat load. In the preparation of a 12 GeV Jefferson Lab experimental
97 proposal on polarized wide-angle Compton Scattering (WACS), a completely new exper-
98 imental approach was developed, based on deploying a high-intensity compact photon

beam source and a polarized target. This new technique opens up physics possibilities that had hitherto been inaccessible at tagged photon facilities and results in a significantly improved figure-of-merit (of a factor of ~ 30) over all previous double-polarization measurements involving photon-induced reactions.

1 Target System and Limitations

The WACS experiment will use a polarized proton target developed by UVA/JLab and typically has been exposed to a beam of 100 nA electrons and provided an averaged proton polarization of approximately 70%. The beam must be moved over the 25 mm face of the target cup to insure that the target material is exposed uniformly to the depolarizing effects of the beam. If the beam were to remain at one location for an extended period it would drill a 'hole' in the target where the polarization had fallen due to local heating and radiation damage. As the NMR system samples the entire target it would, in this case, indicate a much larger value than that where the scattering was taking place. Rastering the beam across the face of the target continuously removes this problem and was made possible in the past by the combination of the standard hall fast raster of ± 2 mm and a specially constructed slow raster. However, the CPS presented here has a very small aperture of 3 mm by 3 mm limiting possible beam motion.

An alternative approach for the beam-target raster is found in Ref. [2] and includes a combination of the target rotation around the horizontal axis and ± 10 mm vertical motion of the target ladder. Such a raster method effectively moves the motion complexity out of the high radiation area of the absorber.

Here we layout the requirements for the rotation and vertical motion which will provide the same uniform exposure as the electron beam raster system used up to now. We start from the premise that the Compact Photon Source (CPS) target system will be able to handle the the same heat load from the photon beam and the microwaves source as used in electron beam experiments. From the perspective of the low energy production of free radicals in the target material, this approximation is expected to be good within 10%. However the free radical complex produced from a high energy beam ($E_{beam} > 20$ MeV) and the way these radicals can effect the polarization is not yet well understood. For now we focus only on the ionization energy loss produced by the multi-GeV photon beam as e^+/e^- pairs. The energy loss from these processes is approximately independent of beam energy and is estimated to be about $2 \text{ MeV g}^{-1} \text{ cm}^2$.

For a photon intensity of 1.5×10^{12} equivalent photons per second it is necessary to use an evaporation refrigerator with ~ 1 Watt cooling power in combination with a high polarization, high radiation resistant proton target material (NH_3). For electron beam experiments typically 100 nA is the maximum current on the target. The heat load in a 3 cm long target can be calculated for NH_3 with density 0.917 g/cm^3 leading to,

$$2[\text{MeVcm}^2/\text{g}](1.6 \times 10^{-13}[\text{J/MeV}])6.25 \times 10^{11}[\text{s}^{-1}](3[\text{cm}])(0.917[\text{g/cm}^3]).$$

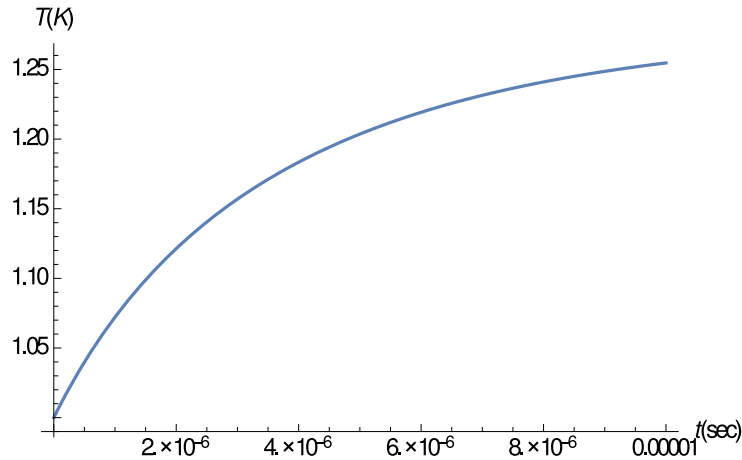
Only about 60% of the ionization energy is actually deposited into the target, leading to about 0.33 Watts. Combined with the heat deposit from microwaves (0.5 W), used to dynamically polarize the target, the cooling power of the UVA/JLab evaporation fridge and pumping system is not saturated. However, cooling power is not the only concern.

135 This heat load must be distributed throughout the target so that the target material
 136 beads are not over-heated on the material boundary so as to create local depolarization.
 137 To do this with electrons a beam rastering system can be used to distribute the beam
 138 over the surface of the target face. The slow raster that spirals out is combined with the
 139 faster raster system which distributes the beam in a 2 mm² square pattern. Our high
 140 intensity photon source is designed to use the fast raster system, however with out also
 141 some sort of slow rastering there would be significant depolarization in the region around
 142 the photon beam spot due to material interfacial thermal heating (ITH).

143 The ionizing radiation inside the target is the primary source of the NH₂ fee radical
 144 but also the ITH. Using simulations with the previously mentioned photon flux and a 2
 145 mm² beam profile leads to 25 nA of ionizing radiation at the exit of the target in an area
 146 of about 6 mm² (containing 90% of the ionizing particles). Taking this spatial distribution
 147 to hold the full 0.33 W heat load from the high intensity photon beam implies that about
 148 100 target beads with an average radius of 1 mm hold all the heat. To calculate the effects
 149 of this heat load on the local polarization we must first start with the heat equation for
 150 a volumetric heat source. This can be expressed as,

$$C_{p0}T^3\rho\frac{dT}{dt} = \dot{Q} - 3R_\alpha\frac{T^4 - T_B^4}{r_{bead}}. \quad (1)$$

151 Using the corresponding values, this equation can be solved with the initial condition
 152 $T(0) = 1K$. \dot{Q} is the volumetric heat load per bead which is conservatively estimated
 153 to be 0.72 W/cm³. Using the specific heat for NH₃ of $C_{p0} = 8.8 \times 10^{-6} \text{ J g}^{-1} \text{ K}^{-4}$,
 154 with ammonia Kapitza resistance $R_\alpha = 1.43 \times 10^{-2} \text{ W cm}^{-2} \text{ K}^{-4}$, with T_B as the liquid
 155 helium bath temperature (1 K), and T is the dynamic material boundary temperature.
 156 The solution to this relation gives the boundary temperature as a function of time and is
 157 shown in Fig 1.



158 Figure 1. Ammonia bead temperature rise due to the beam heat load.

159 These results indicates that after a few microseconds the surface of the bead increases
 160 by about 0.25 K. We can then estimate the time it takes to heat the bead all the way
 161

162 through from the heat on the surface assuming spatial uniformity,

$$\Delta t = \frac{\rho V C_p \Delta T}{\dot{Q}}. \quad (2)$$

163 This calculation results in a time of just a few μs to heat the entire bead from the outer
 164 surface. These times are small on the scale of the time it take for the polarization to
 165 change. To estimate the time it takes to drive the polarization down from the material
 166 beam heating we must consider the DNP rate parameters of NH_3 . This decay time is
 167 related to the microwave power and the spin-lattice relaxation rate. The equations of
 168 motion that give the rate of depolarization can be approximated using the form,

$$\frac{dP(t)}{dt} = \beta T^4 (P_{lim} - P(t)). \quad (3)$$

169 The polarization, limited by the new thermal conditions from Eq. 3, is contained in P_{lim} ,
 170 which is an estimate based on the Brillouin function. The parameter β contains the rate
 171 information and comes from polarization data. The starting polarization of 93% is used
 172 as an example. Solving Eq. 3 numerically results in an approximation of the polarization
 173 drop over time.

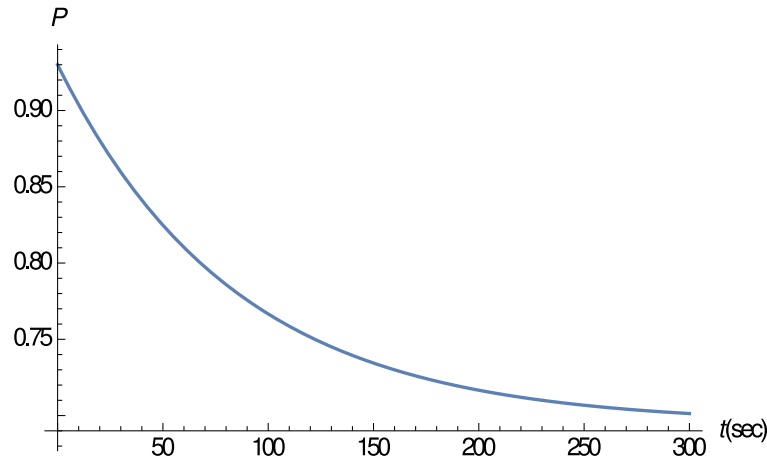


Figure 2. Rotating Target Cup

174

175

176 It is worth noting that calculations here are only estimates and several necessary
 177 parameters required have considerable uncertainty. We use the results as only a guide
 178 to give an order of magnitude check on the time need to rotate the target cell. Figure 2
 179 indicates that the beads should only stay within the same position in the ionizing shower
 180 for no more than a few seconds or the polarization will decrease. This change would not
 181 register in the NMR signal. A rotation on the order of once every few seconds is adequate
 182 for this purpose.

183

The other demand on the target is, of course, the radiation damage induced by all
 184 forms of scattering in the target. If the dose that is mentioned previously (25 nA) from
 185 the ionizing radiation can be distributed over a standard target area of 570 mm^2 , then the
 186 expected depolarization rate from radiation damage is still slower than that of an electron
 187 beam at 100 nA.

188 2 Design of Rotating Target

189 In order to increase the area of the target that the photon beam will interact with a
 190 rotating target was developed to raster photons over the target cup face, see Fig. 3. The
 191 Kel-F target cup is machined to include a gear that can be driven from a rotating shaft
 192 along the target insert. Fig. 3 shows a design of the same dimension of polarized targets
 193 used in the past (2.5 cm diameter by 3 cm length) that fit within the homogeneous field
 194 region of the polarizing 5 T magnet. In the design shown there is no additional material

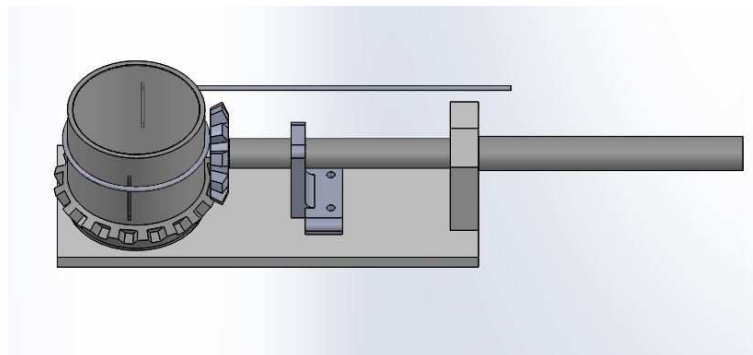


Figure 3. The rotating target cup driven by a gear and shaft with the NMR loop around the
 195 target cell.

196 from the cup in the beam-line. The front and back of the target cell are made of a thin
 197 aluminum foil (not seen in the diagram). The rotation is driven by a gear and shaft. The
 198 NMR couples inductively to the target material by a coil wound around outside of the
 199 cup. The rotating shaft passes through the top of the target insert using a vacuum rotary
 200 feed-through which is then driven by a electric motor.

202 The target rotation in combination with the standard target actuator results in
 203 an effective slow raster which spirals over the full area of the standard 2.5 cm diameter
 204 target. The beam collimation provides the spot size on the target and couples directly to
 205 the resolution characteristics for reconstruction at the cost of holding the beam location
 206 in space fixed. We can still obtain uniform exposure of the target cell by a combined
 207 rotation of the target cup synchronized with an up/down movement of the target ladder.
 208 Rotation of the target cup has already proven viable in many UVA tests. Depolarization
 209 and homogeneous radiation damage can easily be achieved by continuously moving the
 210 target at a rate determined by the radius of the circle made through rotation on the target
 211 surface, spending no more than a few hundred milliseconds on each target location. So
 212 even near the center only 0.01 Hz is required. To avoid mechanical vibration that can
 213 induce noise in the NMR signal it is possible to make several rotations in a fixed diameter
 214 before moving to the next actuator position. This reduces the up and down motion
 215 required to cover the same area. At UVA rotation rates of several Hz have already been
 216 demonstrated. By completing a fixed number of rotations for each experimental run, false
 217 asymmetries and fluctuations from the variations in target bead packing can be averaged
 218 out.

219 III The Compact Photon Source

220 A Conceptual Design

221 A traditional source of bremsstrahlung photons includes a radiator, a deflection
222 magnet with large momentum acceptance, and a beam dump for the used electrons. Such
223 a configuration requires significant space along the beam direction and heavy shielding
224 due to the large openings in the magnet and the beam dump and the many meter length
225 of the system. In addition, it leads to a large size of the photon beam at the target due
226 to divergence of the photon beam and the long path from the radiator to the target. The
227 beam spot size contributes to the angular and momentum reconstruction accuracies of
228 the reaction products which experimentalists want to study. Lastly, it often comes with
229 appreciable radiation doses as particles are allowed to propagate over short distances
230 before mitigation of radiation by containment starts. A new solution for a photon source
231 was proposed in a report at the NPS collaboration meeting in November 2014 about a
232 new experiment for a double polarized wide-angle Compton scattering from the proton at
233 large ($> 3 \text{ GeV}^2$) values of all three kinematical variables s , $-t$, $-u$ (see a detailed analysis
234 of the CPS in Ref. [3]).

235 Reconstruction of the scattered photon depends on multiple factors including the
236 photon spot size at the target. The distance from the radiator to the target is the
237 determining factor here. Studies [1] prepared prior to the WACS proposal submission
238 have shown that spot size of 2mm is well matched to the preserve the benefits of the
239 proton arm angular resolution and the spatial resolution of the photon arm. If needed the
240 distance between the CPS and the target could be increased as it provides an inherent
241 spots size of 0.9 mm.

242 The concept of a new source takes advantage of the narrowness of the photon beam
243 relative to the angular distribution of the secondary particles produced in the electron-
244 nuclei shower. Indeed, the photon beam angular spread, dominated by an electron multi-
245 ple scattering in the $10\%X_o$ radiator, is about $4/E_{beam}[\text{MeV}] \sim 0.4 \text{ mrad}$, but the secondary
246 particles survived filtering through a one nuclear interaction length ($\sim 140\text{-}190 \text{ g/cm}^2$ or
247 $\sim 15 \text{ cm}$) of the heavy absorber, have an angular spread of 0.1-1 radian. The main ele-
248 ments of the CPS are shown in Fig. 4. Without loss of photon intensity, a channel (a
249 collimator for the secondary radiation but not for the photon beam) around the photon
250 beam could be as narrow as the photon beam size with natural divergence plus the size
251 of the beam raster. After passing through the radiator, the electron beam should be
252 removed from the photon line by means of a magnet. The length, aperture and field
253 of the magnet are very different in the proposed source from the traditional one. In the
254 traditional source the magnet is needed to direct the used electrons to the dump. Because
255 of the large momentum spread of used electrons, the magnet aperture needs to be big and
256 the dump entrance should be even bigger (13% of the beam power would be lost before
257 the beam dump, even with a 10% momentum acceptance of the beam line). In contrast,
258 the proposed source has a dump inside the magnet.
259

260 The electron energy dumping starts on the side of the photon beam channel, so a
261 shift of the electron trajectory by just 1-3 mm is already sufficient for the start of the
262 shower. At the same time, such a deflection needs to be accomplished at a relatively

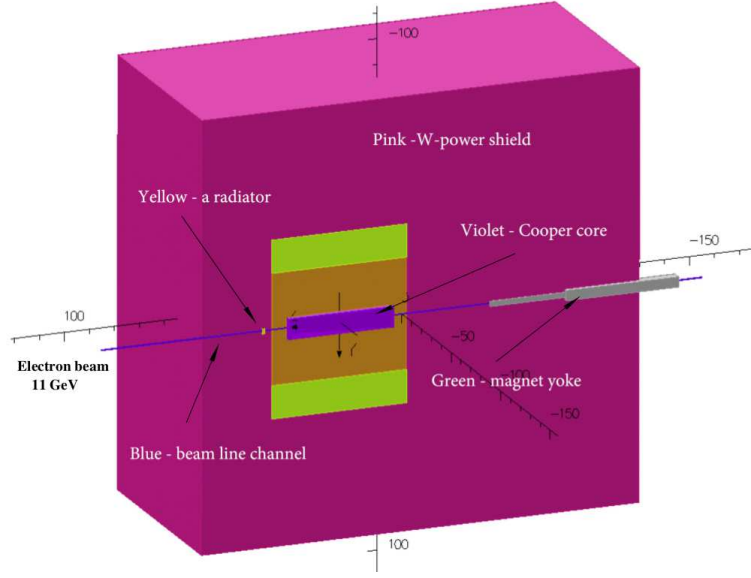


Figure 4. The CPS view.

short distance (much shorter than the size of the radiation shielding) after the beam passes through the radiator to keep the source really compact. Indeed, with a deflection radius, R , a vertical size of the channel, $2a$, and a vertical raster size, $2b$, the trajectory enters the channel side after traveling in the magnetic field the distance, p , which varies from $p = \sqrt{2R(a-b)}$ to $p = \sqrt{2R(a+b)}$ (see the scheme in Fig. 5). In the currently

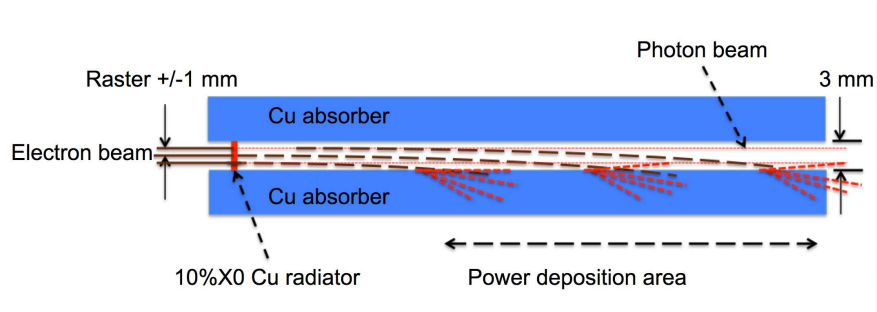


Figure 5. The scheme of beam deflection to the absorber/dump.

268

269

proposed CPS magnet the trajectory radius R is about 10 m for 11 GeV electrons, the channel size is 0.3 cm, and the raster size is 0.2 cm, so the distance p has an average value of 17 cm with a spread of 12 cm. A total field integral of 1000 kG-cm is adequate for our case. It requires a 50 cm long iron dominated magnet.

274

The above concept of the combined magnet-dump allows us to reduce dramatically the magnet aperture and length, as well as the weight of the radiation shield, due to the reduction of the radiation leak through the openings and the short length of the source. This consideration opens a practical way to CPS because it leads to a reduction of power deposition density in the copper absorber.

278

279 B Magnet

280 Normal conducting magnets for high levels of radiation have been constructed at
281 several hadron facilities, e.g. the neutron spallation source at ORNL and the proton
282 complex JPARC. In fact, the radiation level expected in the source allows use of a modest
283 cost kapton tape based insulation of the coils. We designed the magnet with permendur
284 poles taped in two dimensions, which allows us to reach a strong magnetic field (3.2 Tesla)
285 at the upstream end of the magnet, and moved the coils to 20+ cm from the source of
286 radiation. The length of the magnet was selected to be 50 cm and the field integral 1000
287 kG-cm (see the field profile). Figure 6 shows the longitudinal profile of the magnetic field
288 according to the OPERA calculation.

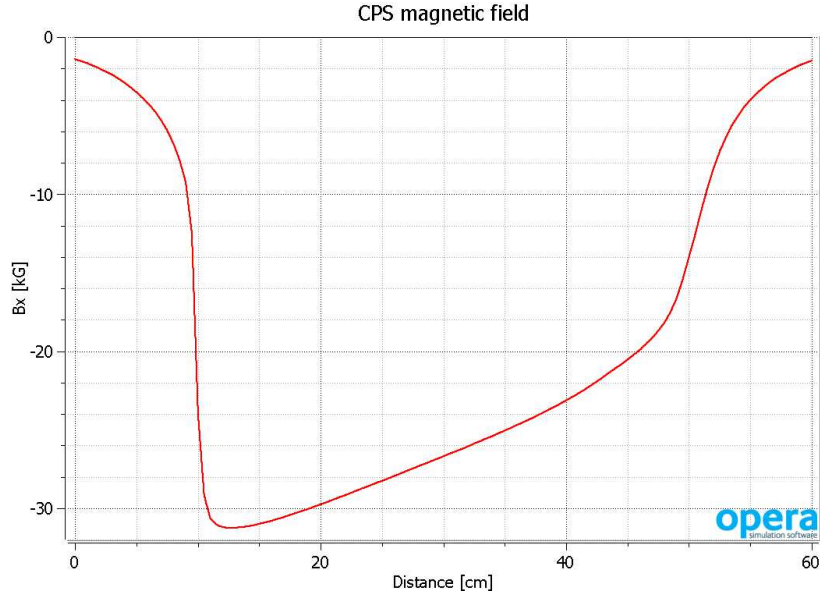


Figure 6. Magnetic field (B_x) profile along the beam direction.

291 C Central absorber

292 The beam power absorber will be made of copper, whose high heat conductivity
293 helps to manage the power density. If it is needed, we can use an aluminum absorber,
294 which would help to reduce power density even more by a factor of 2-3 due to a six times
295 larger radiation length, but it would also increase the length of the source by about 50 cm.
296 The heat removal from the copper absorber is arranged first via heat conductivity to the
297 wider area where the water cooling tubes are located. At 10-15 cm from the beam line, the
298 temperature of the copper insert drops to a level below 100°C (the calculation of the energy
299 deposition was made in both the SIMC and Geant4 frameworks, and the temperature 2-
300 dimensional analysis was performed for the highest power density area). Figure 7 shows
302 the longitudinal profile of the power density according to the MC simulation.

303 The transverse distribution of power is also very important to take into account
304 because, for a high energy incident beam, it has a narrow peak. A detailed MC simulation

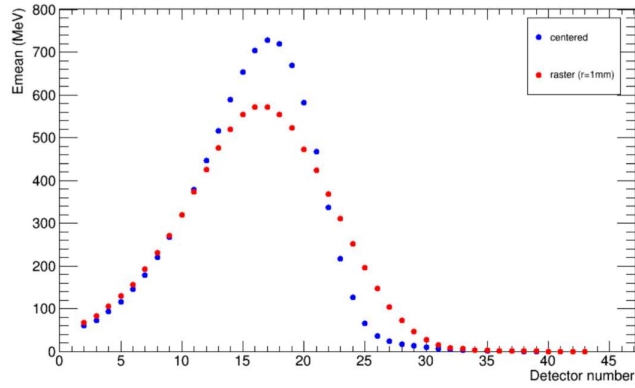


Figure 7. Longitudinal profile of the power distribution (integrated for one cm copper slab) for one 11 GeV incident electron. The maximum power density is at the coordinate 18 cm. The blue dots show the energy deposition for the electron beam centered in a 3 mm by 3 mm channel. The red dots show the same for the beam rastered with a radius of one mm.

of power density and 2-dimentional heat flow analysis were performed to evaluate the maximum temperature in the copper absorber. Temperature was found to be below 400°C, which is well in the acceptable range for copper (the calculation was performed for the case of a 11 GeV 30 kW beam and a 10% X0 radiator). Figure 8 shows the temperature profile in the transverse plane at the longitudinal location of maximum power deposition. Cooling of the core will require about four gallons of water per minute at 110 psi pressure

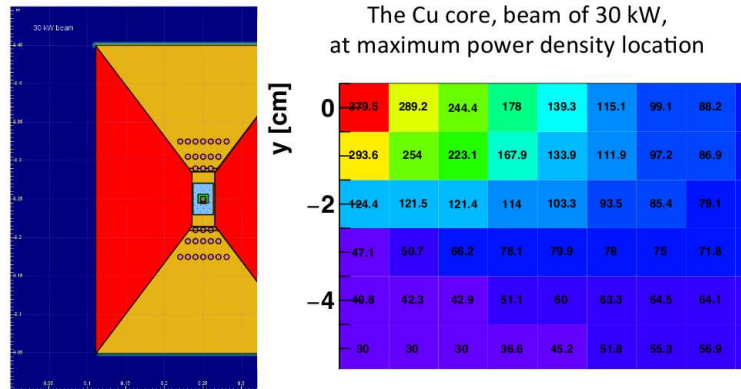


Figure 8. The cross section of the absorber (shown by yellow and blue in the center) with the cooling channels and the temperature map.

(at 30°C temperature rise), which is easy to provide.

314 D W-powder shield

315 The amount of material needed for radiation shielding is defined by the neutron
 316 attenuation length, which is 30 g/cm^2 (for neutrons with energy below 20 MeV) and
 317 125 g/cm^2 (for high energy neutrons, see in PDG). The neutron production rate by an
 318 electron beam in copper is 1×10^{12} per kW of beam power according to the SLAC report
 319 (W.P. Swanson, SLAC-PUB 2042, 1977, see Fig. 9). At a distance of 16 meters from the
 320 unshielded source for a 30 kW beam, the neutron flux would be $1 \times 10^7 \text{ n/cm}^2/\text{s}$, which
 321 would produce a radiation level of 110 rem/h, or 850 times higher than during the RCS
 322 experiment (at a 16-meter distance from the pivot in the upstream direction). A radiation
 323 reduction factor of 1000 will be achieved by means of a shield with a mass of 850 g/cm^2 .
 324 For the shield outside the magnet, the current design uses tungsten powder, whose high
 325 density (16.3 g/cm^3) helps to reduce the total weight of the device. A thickness of 50 cm
 326 was used as a first estimate for the thickness of the outer shield in CPS.

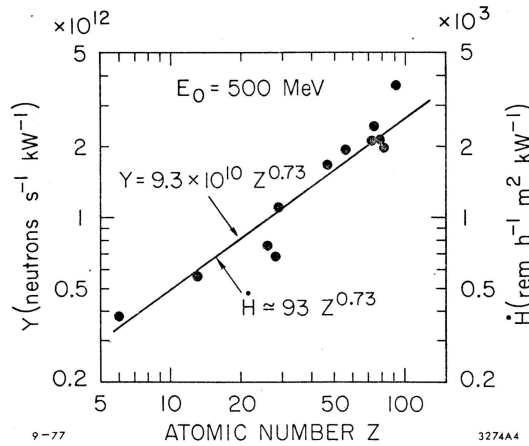


Fig. 12

Figure 9. The neutron yield according to Swanson's report.

329 IV Radiation Requirements

330 The goal of the Compact Photon Source is to convert beam energies of up to 12 GeV
 331 with currents of up to $5 \mu\text{A}$ into a high-intensity source of collimated photons. For the
 332 Hall-D adaptation, the $5 \mu\text{A}$ beam current is limited by the design of the Hall D Tagger
 333 Magnet alcove. This corresponds to a 60 kW power limit. For the Halls A/C adaptation,
 334 the beam energy is limited to 11 GeV. Many experiments will opt to use the traditional
 335 method for photon beam experiments, with the high-current electron beam striking a 10%
 336 radiation length Cu radiator. The Compact Photon Sources gain in Halls A/C is foreseen
 337 for use with Dynamically Nuclear Polarized targets. Electron beam currents for use with
 338 such targets is typically limited to 100 nA or less, to reduce heat loading and radiation
 339 damage effects. The equivalent heat load for a pure photon beam impinging such targets
 340 corresponds to a photon flux originating from a $2.7 \mu\text{A}$ electron beam current striking a

341 10% Cu radiator. Hence, the Compact Photon Source design for Halls A/C should be
 342 able to absorb 30 kW in total (corresponding to 11 GeV beam energy and 2.7 μ A beam
 343 current).

344 In addition, the typical beam time we assume for an approved experiment at Jeffer-
 345 son Lab is 1000 hours (\approx 40 PAC days). For such a Compact Photon Source experiment,
 346 one needs to fulfill the following radiation requirements:

- 347 • Prompt dose rate in hall \leq several rem/h at 30 feet from device.
- 348 • Prompt dose rate at the site boundary \leq 1 μ rem/r (2.4 μ rem/h corresponds to a
 349 typical experiment at Jefferson Lab not requiring extra shielding).
- 350 • Activation dose outside the device envelope at one foot distance is \leq several mrem/h
 351 after one hour following the end of a 1000 hour run.
- 352 • Activation dose at the pivot in the experimental target area, where operational
 353 maintenance tasks may be required, is dominated by the dose induced by a pure pho-
 354 ton beam, and at one foot distance from the scattering chamber \leq several mrem/h
 355 after one hour following the end of a 1000 hour run. *i.e.*, the additional dose in-
 356 duced by radiation of the main beam absorbed in the Compact Photon Source is
 357 negligible.

358 The Compact Photon Source design should combine in a single properly shielded
 359 assembly all elements necessary for the production of the intense photon beam, including
 360 that the operational radiation dose rates around it are acceptable as outlined in the re-
 361 quirements above. Much of this is achieved by keeping the overall dimensions of the setup
 362 limited, and by shielding induced radiation doses as close to the source as possible, and by
 363 careful choice of materials. Compared to the traditional bremsstrahlung photon source,
 364 the proposed solution will present several advantages, including much lower radiation lev-
 365 els, both prompt and post-operational due to the beam line elements radio-activation, as
 366 will be shown later.

367 The Compact Photon Source conceptual design has been established with extensive
 368 and realistic simulations. As validation of the simulation tools used, we have also per-
 369 formed a benchmark comparison using tools such as GEANT3, GEANT4, FLUKA and
 370 DINREG. The benchmark results are further described in Appendix B. After benchmark
 371 validation, we have performed an extensive series of radiation calculations to:

- 372 • Determine the size and layering of the shielding around the magnet, and the choice
 373 of materials (Cu, Cu-W alloy, concrete, borated plastic, etc.).
- 374 • Determine the magnet field requirements in terms of peak field, gap size, and field
 375 length.
- 376 • Determine the radiation level on the magnet coils and based on these results identify
 377 radiation hardened materials that might be used in building the coils.
- 378 • Determine the radiation level on the polarized target electronics.
- 379 • Determine the radiation level immediately next to the device as well as at the
 380 experimental hall boundary.

381 The logic behind the CPS hermetic shielding design is that radiation (γ , n) from
 382 the source should be a few times less than from a photon beam interaction with the
 383 material of a polarized target. The CPS is designed to meet the acceptable radiation
 384 level requirements specified in Appendix 2 for electron beam current of $2.7\mu\text{A}$ (30 kW),
 385 run time of 1000 hours, and the photon source as close to the target as possible. The
 386 shielding design consists of tungsten powder and 10cm of 30% borated plastic. The
 387 addition of the latter has considerable impact in reducing the neutron flux, illustrated in
 388 Figure 13.

389 V Radiation Studies and Shielding Design

390 In this Section we will describe several different configurations for comparison. One
 391 is what has been the default situation for Dynamically Nuclear Polarized targets in Hall C
 392 and elsewhere, assuming an up to 100 nA electron beam current we call this scenario "100
 393 nA electron beam". A second configuration is the equivalent photon flux created by a 2.7
 394 μA electron beam on a 10% Cu radiator, impinging on the same polarized target system.
 395 Here, we removed all the secondary particles generated, so this situation mimics a pure
 396 and background-free photon beam. This scenario is called " $2.7\mu\text{A}$ photon beam". The
 397 third scenario is that with the CPS (Compact Photon Source), under the same conditions:
 398 a $2.7\mu\text{A}$ electron beam strikes a 10% Cu radiator. Here, all the radiation background is
 399 taken into account and simulated. In some cases we have simulated only the effect of the
 400 CPS, in some cases the CPS and the target system combined. These scenarios are called
 401 "CPS", or "CPS with Polarized Target".

402 1 Prompt Radiation Doses (without a Target)

403 To explain the shielding concept of the CPS, we start with comparing the prompt
 404 radiation doses as calculated in a ring detector which covers a range between 5 and 10
 405 cm radius from the beam line. This such that we could directly compare GEANT and
 406 FLUKA calculations.

408 We first calculate the prompt doses originating from a $2.7\mu\text{A}$ electron beam hitting
 409 a 10% Cu radiator a distance of 2.15 meter before the pivot. There is no target system in
 410 this simulation, and all prompt radiation originates from the Cu radiator. Figure 10 shows
 411 two-dimensional dose rates as originating from photons only (top left), from neutrons only
 412 (top right), from all particles (bottom left) and the (one-dimensional) prompt radiation
 413 dose along the beam direction (bottom right). Obviously, most prompt radiation is created
 414 along the beam direction, although this is less obvious from the neutron-only figure.
 415 The prompt radiation levels reach roughly 40 rem/hour. Interestingly, the gamma-only
 416 contribution only amounts to roughly 200 mrem/hour, and the neutron-only is less than
 417 10 mrem/hour. They together fail to account for the total prompt radiation simulated
 418 along the beam line. That there is another contribution can readily be seen from the
 419 bottom right panel, which shows another source of prompt radiation coming in these are
 420 the charged electrons and positrons created, inducing further showers.

422 A striking difference is observed for the same situation, a $2.7\mu\text{A}$ electron beam

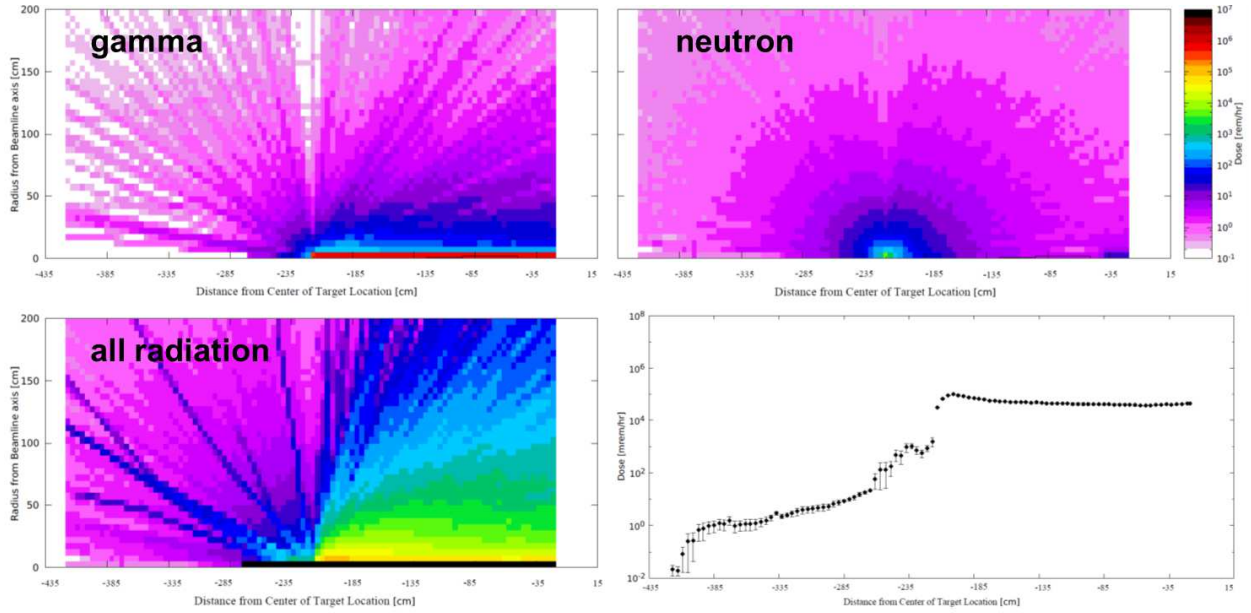


Figure 10. Two-dimensional dose rates as originating from photons only (top left), from neutrons only (top right), from all particles (bottom left) and the (one-dimensional) prompt radiation dose along the beam direction (bottom right).

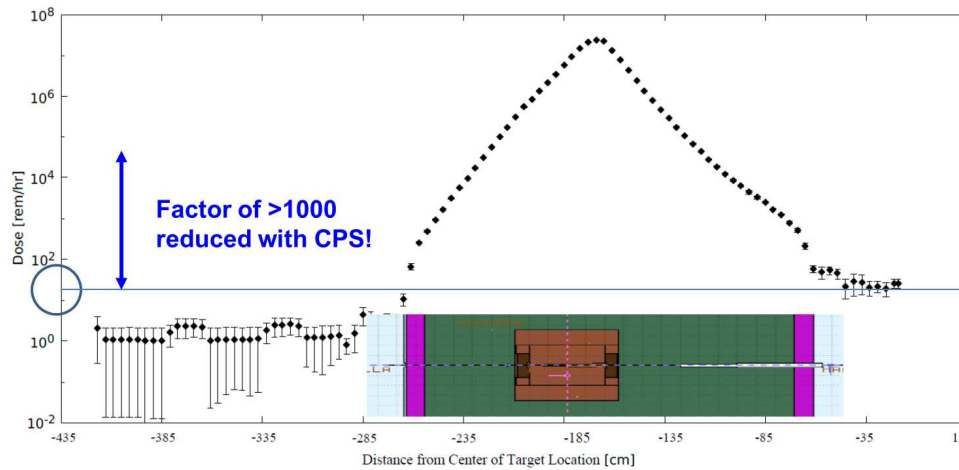


Figure 11. Two-dimensional dose rates as originating from photons only (top left), from neutrons only (top right), from all particles (bottom left) and the (one-dimensional) prompt radiation dose along the beam direction (bottom right)..

423 hitting a 10% Cu radiator, but now within the CPS. Figure 11 illustrates the prompt
 424 radiation dose along the beam direction. The scales of this Figure are consistent with
 425 those in Figure 10 (bottom right panel). One can see the prompt radiation (again, in a 5
 426 to 10 cm ring detector along the beam axis) within the CPS is much higher, but outside
 427 the CPS the prompt radiation dose is reduced to roughly 15 mrem/hour, a reduction
 428 by over a factor of 1000! This factor is entirely consistent with the predicted radiation

reduction factor of Section III D.

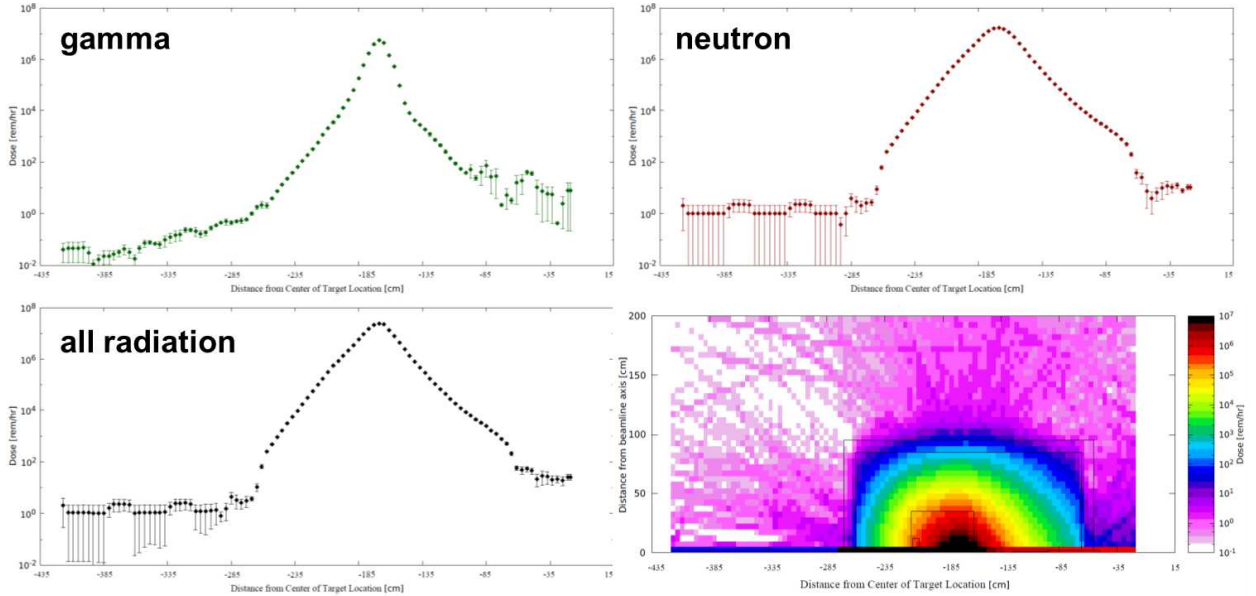


Figure 12. The (one-dimensional) prompt radiation rates as originating from photons only (top left), from neutrons only (top right), and from all radiation sources (bottom left). The fourth panel (bottom right) illustrates how well an optimized CPS shielding concept absorbs the prompt radiation, outside the CPS the prompt radiation is on the surface (indicated by the outer black rectangular lines) already reduced to a level of roughly 10 rem/hour at most.

Why this magic? This is further illustrated in Figure 12. In the first three panels we show the (one-dimensional) prompt radiation rates as originating from photons only (top left), from neutrons only (top right), and from all radiation sources (bottom left). In striking contrast with the case without CPS, there is no contribution from photons, electrons, and positrons anymore: the neutron-only calculation is near-identical to the all-radiation-calculation. The fourth panel, Figure 12 (bottom right) illustrates how well an optimized CPS shielding concept absorbs the prompt radiation, outside the CPS the prompt radiation is on the surface (indicated by the outer black rectangular lines) already reduced to a level of roughly 10 rem/hour at most. The shielding concept works so well as showers never get a chance to develop and photons are contained. There will always neutrons leak out.

This indirectly confirms that with a CPS the prompt dose rates in the hall can easily obey the following requirement: **Prompt dose rate in hall \leq several rem/h at 30 feet from device.**

2 Impact of Boron and Shielding Optimization

It is well known that the neutron fluences can be drastically reduced by the addition of boron, which acts as an excellent capture material for low-energy neutrons. We simulated this property ourselves by calculating the neutron flux at the CPS boundary

450 assuming various thicknesses of tungsten shielding (65, 75 and 85 cm radial), and then
 451 adding 10 cm of borated (30%) plastic. The result can be seen in Figure 13, showing
 452 the neutron flux as function of neutron energy (on a logarithmic scale). Adding 10 cm
 453 of tungsten reduces the neutron flux, but a much more drastic reduction is seen when
 454 adding the 10 cm of borated plastic. Thus, in our design we assume an outer layer of the
 455 CPS, beyond the tungsten powder, of borated plastic with a thickness of 10 cm.

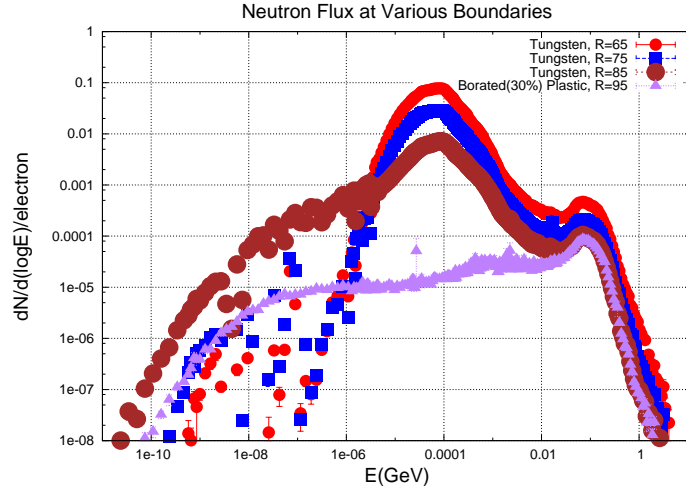


Figure 13. Impact of boron on shielding properties.

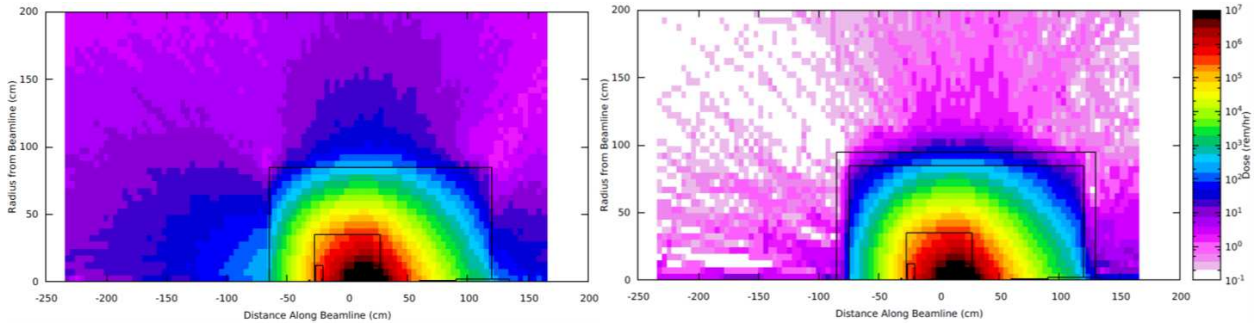


Figure 14. The prompt radiation rates with the optimized shielding design, whereas in the left
 panel we show the same prompt radiation rates without extra shielding (10 cm less of tungsten
 shielding, and no borated plastic). Note: these are with the CPS magnet centered around "zero"
 along the beam line.

458 That our shielding design has been optimized well can be further exemplified in
 459 Figure 14. In the right panel we show the prompt radiation rates with the optimized
 460 shielding design, whereas in the left panel we show the same prompt radiation rates if
 461 we would have had 10 cm less of tungsten shielding, and no borated plastic. The effect
 462 is remarkable, one readily can witness much higher prompt radiation rates escaping the
 463 CPS. But this also shows our CPS shielding design is well optimized! Please do note that
 464 in these panels the CPS magnet is assumed to be at the center (zero distance) along the
 465 beam line, in contrast with earlier Figures.

466 3 Prompt Dose Rates at the Boundary

467 In benchmark calculations assuming spheres of pure shielding materials (see a more
468 extensive description of the benchmark calculations in Appendix VIB 10) we find that
469 the prompt dose rate estimates at the RBM-3 boundary are $0.24 \mu\text{rem}/\text{hour}$ for a 3 meter
470 (diameter) iron sphere and $2.4 \mu\text{R}/\text{hour}$ for a 1.5 meter (diameter) tungsten sphere.

471 Our typical CPS shielding is assumed to be 85 cm thick radially and surrounded by
472 10 cm or borated plastic. Hence, the boundary dose is tuned below the $2.4 \mu\text{rem}/\text{hour}$ that
473 corresponds to a typical experimental run at Jefferson Lab not requiring local shielding per
474 the radiation budget. So, we are already **below the level of $2.4 \mu\text{rem}/\text{h}$ corresponds**
475 **to a typical experiment at Jefferson Lab not requiring extra shielding**. With
476 further choice of proper material and ordering, the boundary dose can be tuned even
477 further down, as required.

478 We do note that for Hall D the CPS design is compatible with the site boundary
479 as the conditions for the regular Hall D tagger magnet operation can dump up to 60 kW
480 in a local beam dump: the Hall D tagger building has been designed assuming an up to
481 12 GeV beam energy and an up to $5 \mu\text{A}$ electron beam current. For the CPS, one can
482 thus assume the Hall D tagger magnet building shielding is appropriate also when up to
483 60 kW is dumped in the CPS itself. Additional local shielding may be required.

484 4 Activation Doses (without a Target)

485 We now turn to the activation doses expected around the CPS. Figure 15 shows
486 the calculated activation dose one hour after a 1000-hour experiment under the described
487 conditions ($2.7 \mu\text{A}$, 10% Cu radiator, with shielded CPS) has been completed. Please note
488 again that in this Figure the CPS magnet is assumed to be at the center (zero distance)
489 along the beam line. The radiation calculations show the activation dose outside the CPS
490 is reduced to the order of roughly $1 \text{ mrem}/\text{hour}$. To quantify this further, Figure 16 shows
491 the activation dose radially away from the CPS. The activation dose outside the CPS is,
492 one hour after a 1000-hour run, reduced to $2 \text{ mrem}/\text{hour}$ on contact and reduces radially
493 outward. At one-foot distance, it is reduced to about $1.5 \text{ mrem}/\text{hour}$, and at two-feet
494 distance to less than $1 \text{ mrem}/\text{hour}$.

496 Hence, this easily fulfills the requirement that **Activation dose outside the de-**
497 **vice envelope at one foot distance is \leq several mrem/h after one hour following**
498 **the end of a 1000 hour run.**

499 Note that these estimates do not depend much on the assumed 1000-hour continu-
500 ous run, we also simulated a 100-hour continuous run but the activation doses are, albeit
501 slightly smaller, nearly the same, reflecting that much of the activation is instant. Ac-
502 tivation doses also do not drop appreciably drop if one waits one hour or one day. On
503 the other hand, if one would wait a week or a month the activation doses at contact
504 can be reduced by up to a factor of ten. Inside the CPS, the activation doses can be
505 up to $1 \text{ Krem}/\text{hour}$, which is why we will move the CPS laterally to the side in between
506 experiments, with rails on a stand, and do not disassemble.

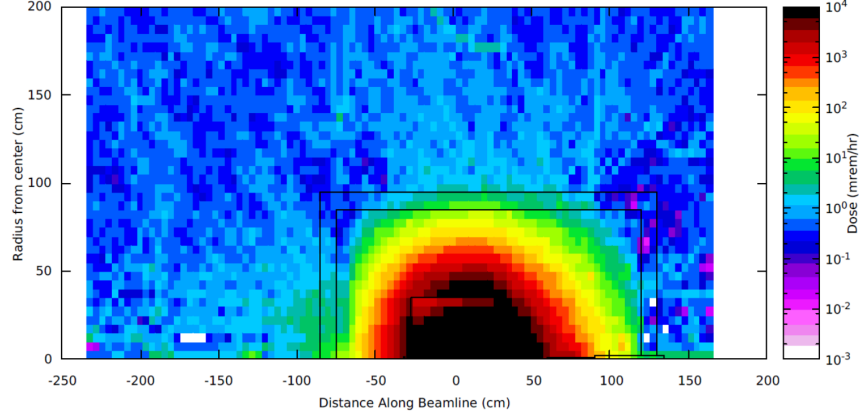


Figure 15. Calculated activation dose one hour after a 1000-hour experiment under the described conditions ($2.7 \mu\text{A}$, 10% Cu radiator, with shielded CPS) has been completed. Note: these are with the CPS magnet centered around "zero" along the beam line.

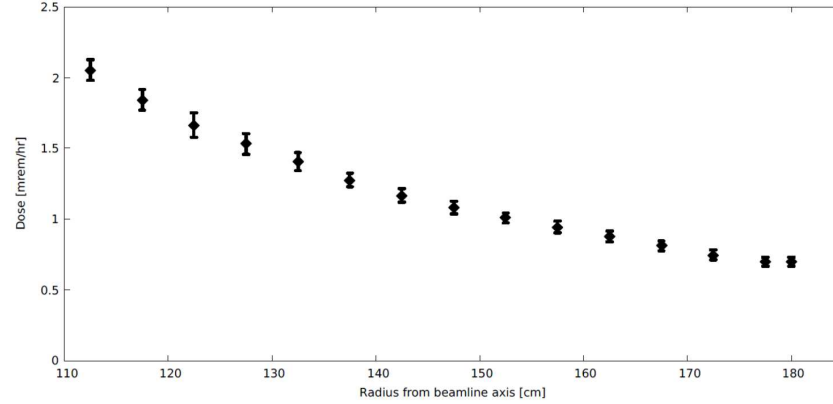


Figure 16. Activation dose outside CPS 1 hour after a 1000 hour run is 2 mr/hr on contact and reduced radially outwards.

507 5 Radiation Doses with a Target

508 In the further radiation calculations, we have also included the polarized target
 509 scattering chamber and target system. In Figure 17 we illustrate our setup and show a
 510 side view of the Compact Photon Source, indicating the magnet, the W powder shield,
 511 and the layer of borated plastic, and also the scattering chamber with polarized target
 512 system. The description of the scattering chamber and polarized target includes: (i) the
 513 exact diameter of the scattering chamber and all the ports with their exact dimensions
 514 and window materials, and (ii) the polarized target material but also the liquid helium
 515 surrounding the target beads, etc.

516 We add Figure 18 for completeness, it illustrates the 1-MeV neutron equivalent
 517 damage to silicon (in neutrons/cm²). This is the relevant quantity to use to outline
 518 when one has to worry about radiation damage to sensitive electronics. The result, not
 519 surprisingly, shows that there is a narrow cone in the forward direction, along the beam

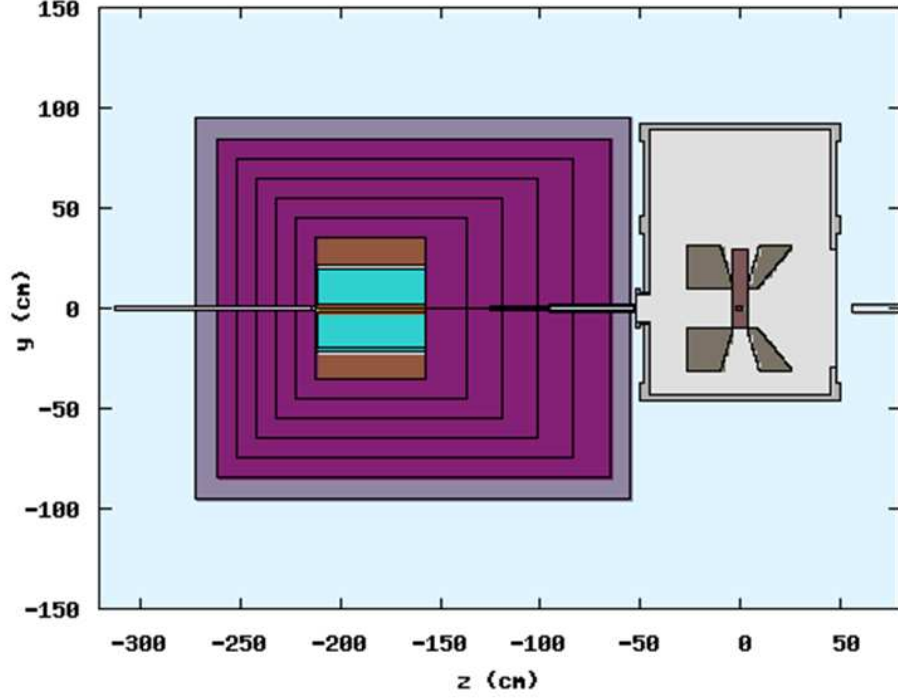


Figure 17. Side view of the Compact Photon Source, indicating the magnet, the W powder shield, and the layer of borated plastic, and also the scattering chamber with polarized target system.

axis, up to roughly one meter, that should be evaded for electronics.

Figure 19 shows the prompt dose at the target for different configurations. The distance R is radial distance from the pivot, with the radius of the scattering chamber boundary at 50 cm. The various calculations reflect the "100 nA electron beam" (red downward triangles), the "2.7 μ A photon beam" (blue upward triangles), the "CPS" (without polarized target, black circles), and the "CPS with Polarized Target" (mauve squares). At the boundary of the scattering chamber, the "100 nA electron beam" configuration, the default operating mode for polarized beam experiments with dynamically nuclear polarized targets to date in Hall C, the prompt dose is roughly 1 rem/hour. The "2.7 μ A photon beam" scenario is roughly 30 rem/hour. This simply reflects that even if a 2.7 μ A pure photon beam deposits the same heat load in a target as a 100 nA electron beam, the radiation rate is much higher. The "CPS with Polarized Target" scenario is identical to the pure photon beam. Hence, no additional radiation comes from the CPS, it is well shielded.

Figure 20 is perhaps more instructional, in that it shows the activation dose rates for three configurations, "100 nA electron beam" (left), "2.7 μ A photon beam" (middle), and "CPS" (without polarized target, right). The figure panels have different vertical size, such that equal dose rates line up from left to right. One directly can see that the "2.7 μ A photon beam" configuration has much higher activation doses than the "100 nA electron beam". This again reflects what was seen in Figure 19 also for prompt radiation dose rates, there are a large amount of more photons coming from a 2.7 μ A electron beam

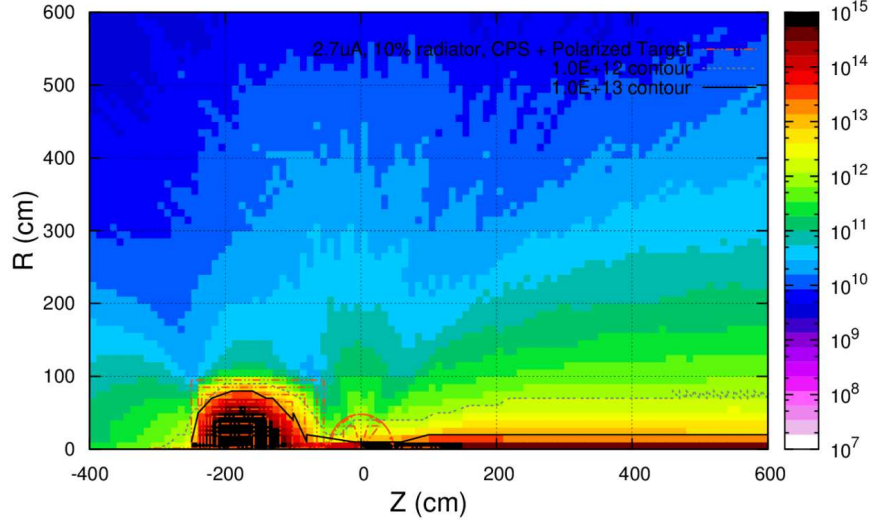


Figure 18. 1-MeV neutron equivalent damage to silicon (in neutrons/cm²).

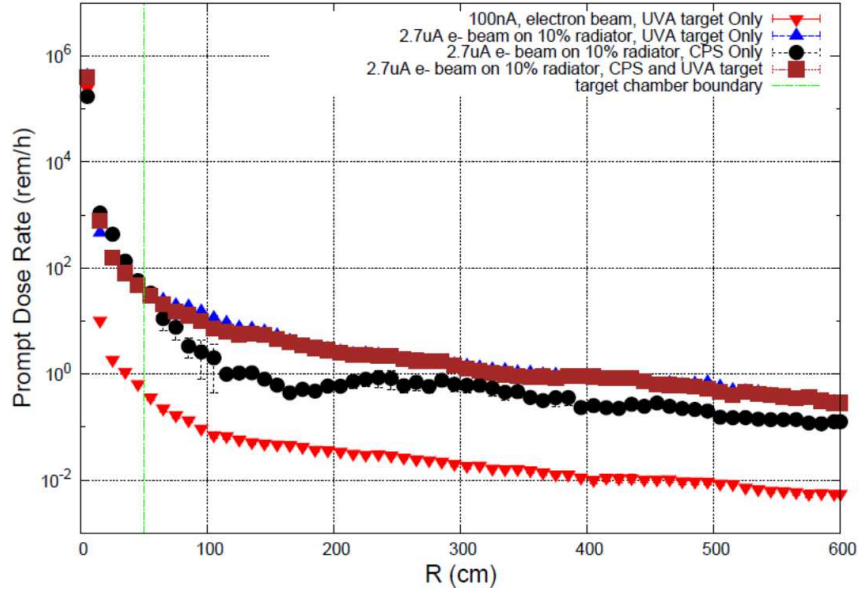


Figure 19. Prompt dose at the target for different configurations. Distance R is radial distance from the pivot, with the radius of the scattering chamber boundary at 50 cm.

on a 10% Cu (radiator) target than there are from a 100 nA electron beam on a roughly
 3% dynamically nuclear polarized target (we assumed NH₃). More interestingly, the effect
 of the CPS is negligible: activation near the target does not come from the CPS itself,
 it rather comes from the powerful photon beam we have created. The price to pay is
 that one ends up with a roughly constant 0.1 mrem/hour activation level at large radial
 distances, but this is negligible.

We also indicate in the various panels how fast the activation decays, and indicate
 levels after 1 hour, 1 day, 1 week, and 1 month. One can see that the 0.1 mem/hour

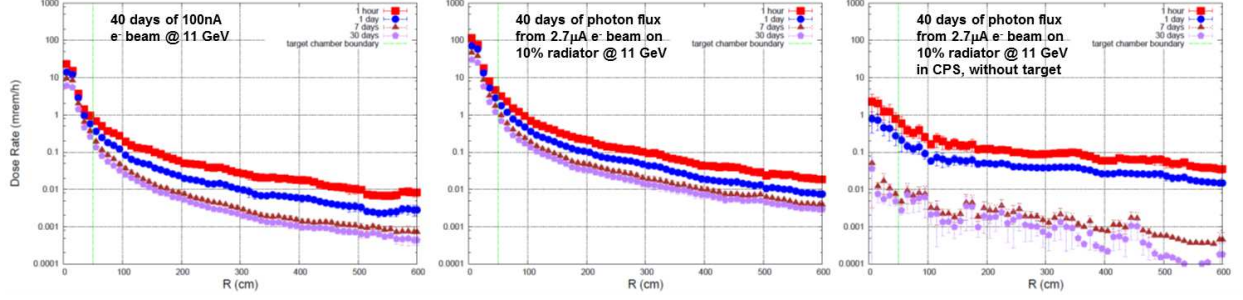


Figure 20. Activation dose rates at the target for different configurations. Distance R is radial distance from the pivot, with the radius of the scattering chamber boundary at 50 cm.

549 activation level one has induced by the use of the CPS has a long life-time but has
 550 decayed away after a week. This is consistent with what was observed in the example of
 551 the activation levels at radial distances around the CPS above.

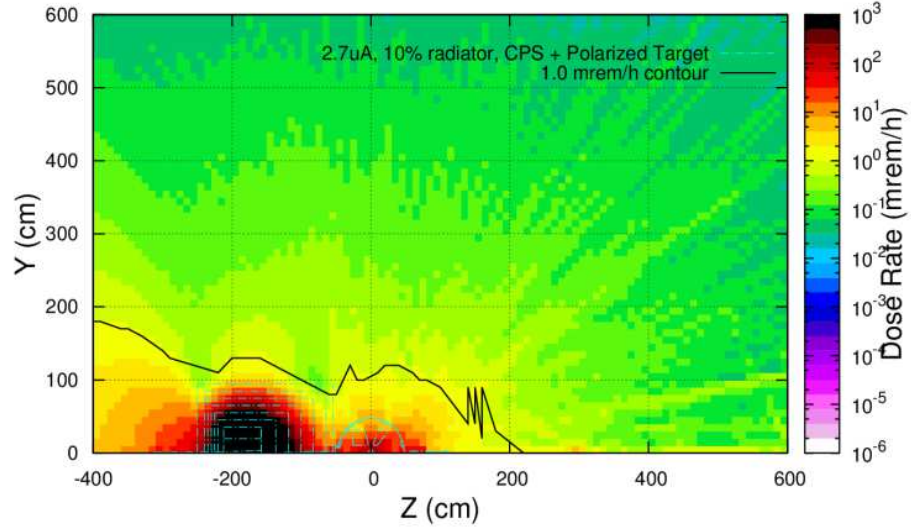


Figure 21. Activation dose rates one hour after a 1000 hour run with the Compact Photon Source, a $2.7 \mu\text{A}$ beam and a 10% radiator, at 11 GeV beam energy, and the polarized target system (at $z = 0$). The 1 mr/hr contour is indicated.

552 Lastly, we illustrate in Figure 21 in a two-dimensional plot the activation dose rates
 553 one hour after a 1000 hour run with the Compact Photon Source, with a $2.7 \mu\text{A}$ beam
 554 and a 10% radiator and an 11-GeV electron beam energy, and the polarized target system
 555 (at $z = 0$). The 1 mrem/hour contour is indicated.

556 This proves that with the well-shielded CPS design, the **Activation dose at the**
 557 **pivot in the experimental target area, where operational maintenance tasks**
 558 **may be required, is dominated by the dose induced by a pure photon beam and**
 559 **is at one-foot distance from the scattering chamber \leq several mrem/h after**
 560 **one hour following the end of a 1000 hour run, and also that the additional**
 561 **dose induced by radiation of the main beam absorbed in the Compact Photon**

562 **Source is negligible.** This was the last of the radiation requirements put forward in
563 Section ??.

564 **VI Safety and Engineering Aspects**

565 **A Safety**

566 Realization of the proposed device will boost the experiment productivity by a factor
567 of 30 but it is relatively expensive and require especially reliable construction methods.
568 From safety point of view the CPS device is a modest power (30 kW) beam dump installed
569 in a middle of the hall. There are several safety aspects in this project. Here we show a
570 list for a full scope including items which are already analyzed in the previous sections
571 of this document and a few others which will be considered in details in future stages of
572 development.

- 573 • Prompt radiation level in the hall
- 574 • Radiation level at the JLab boundary
- 575 • Residual radiation in the hall
- 576 • Radiation level at the polarized target coils (both prompt and residual)
- 577 • Radiation level at the detector electronics
- 578 • Radiation level at the magnet coils and absorber cooling water
- 579 • Radiation aspects after experiment completion
- 580 • Safety documentation, review, and approvals

581 The current results are based on the studies of the radiation levels using FLUKA
582 (also comparison with Geant4) and comparison with the data from several experiments
583 already performed at JLab. Regarding first two items we found that levels of radiation is
584 well below typical for high luminosity experiments in Hall C or A. The residual radiation
585 on the surface of CPS is of a few mrem/h after 100 hours cooling. Radiation on the CPS
586 magnet coils was found to be of 80 kRad/h, see Ref. [3], page 19. Prompt radiation level
587 on the polarized target coils is about 150 rem/h due to interaction of the photon beam
588 with the material of the polarized target.

590 **B Engineering**

591 The CPS device is a specialized beam dump but many considerations for the design
592 are similar to the medium power dumps constructed at Jefferson Lab, see e.g. Ref. [4]. In
593 addition to the radiation and power handling considerations we need to take into account
594 short term nature of CPS installation for just one or several experiments, which requires
595 removal of the activated system from the beam line soon after experiment completion.

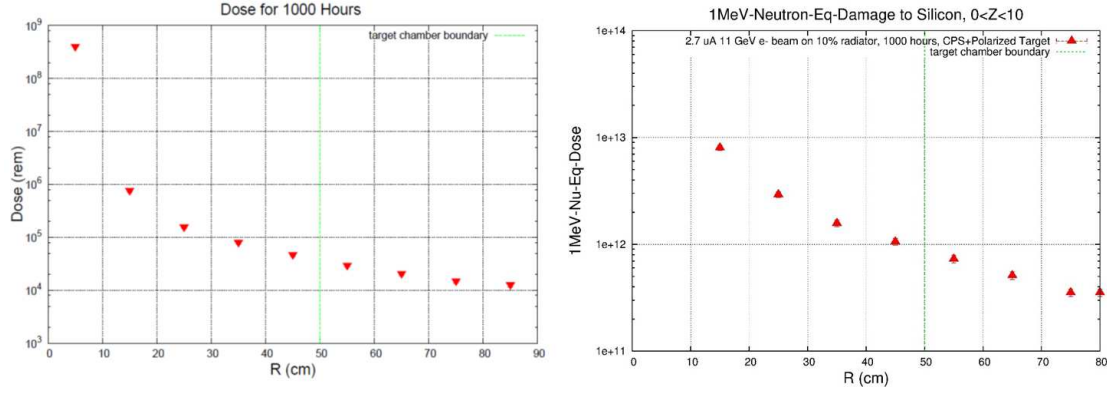


Figure 22. The prompt dose rates (right) and the resulting 1 MeV neutron equivalent damage to silicon (left) in the target area, assuming a 1000 hour run with the Compact Photon Source with a 2.7 mA beam, a 10% Cu radiator, and 11 GeV beam energy. The polarized target system is at $z = 0$ and the nominal target chamber radius is 50 cm. The target coils are at about 20 cm from the beam line. The dose for 1000 hours of beam time at the target coils is 5 times 10^5 rem and the 1 MeV neutron equivalent damage is 5 times 10^{12} neutrons/cm². The contribution of the CPS backgrounds to these numbers is negligible (contributing 2.5% only).

596 The CPS is planned to be installed 5 meters upstream of the hall pivot and the polar-
 597 ized target 7 meters from usual location because the experiment does not use SHMS/HMS
 598 but both detector arms (NPS and BigBite) will have custom support frames. The NPS
 599 and Bigbite will be located on the floor between SHMS and HMS as close as feasible to
 600 the present Hall C Pivot.

601 The CPS will be installed in the area upstream of the Hall C pivot which is already
 602 occupied by several Hall C systems. The final Hall C girder containing BPMs, BCMs,
 603 correctors and other devices will have to be significantly modified. The cost for this
 604 modification and remount of the instrumentation must be estimated and included in the
 605 experiment total. The downstream portion of this girder is cantilevered over the SHMS
 606 data cable hoses which arc around the pivot and permit rotation. The SHMS Data hoses
 607 cannot be removed or significantly modified. They do permit legs for the CPS stand.
 608 These legs may limit the freedom of SHMS rotation somewhat.

610 There were considered the following engineering aspects in the CPS project:

- 611 • Forces from the closely located magnets
- 612 • Modification and rebuild of the Hall C final instrumentation girder
- 613 • Installation/survey of CPS on the beam line
- 614 • Fast raster trip detection and raster interlock
- 615 • Interlock system: temperatures, radiation, water flow
- 616 • Commissioning plan including some engineering tests
- 617 • Removal of the CPS from the beam line after the experiment

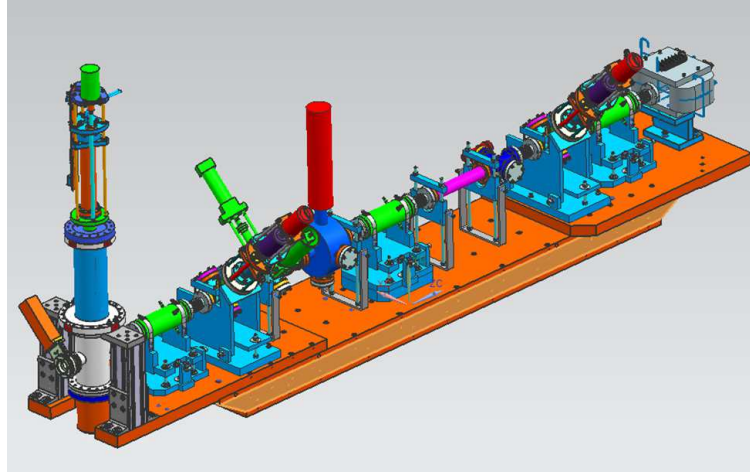


Figure 23. The present final girder in Hall C.

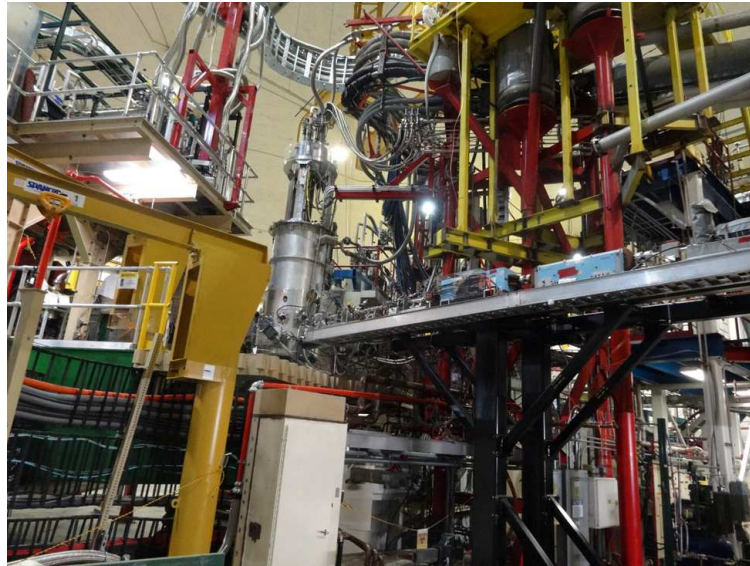


Figure 24. Final Hall C girder, SHMS data cable hoses and environment.

- 618 • Safety documentation, review, and approvals
- 619 • Preliminary cost estimate

620 1 Magnetic Forces and Gradients at the Polarized Target

621 The CPS magnet will be located relatively close to the 5 Tesla solenoid of the polar-
 622 ized target whose mutual forces need to be taken into account in the design of the support
 623 structure and may require compensation. Preliminary analysis was already performed in
 624 the technical note in 2015 for iron-based shielding which currently replaced by W-power
 625 which reduced forces very much. Residual fields and forces from the CPS magnet will

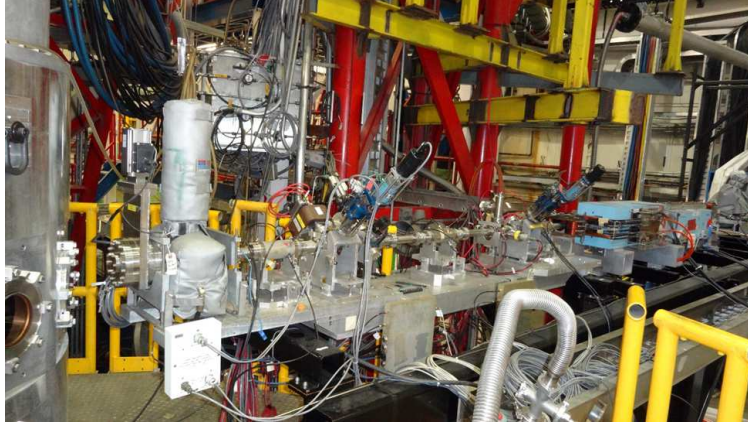


Figure 25. Closer view on final Hall C girder.

require iron shielding to avoid interference with the Polarized Target magnet. Another magnetic consideration is the effect on field quality at the polarized target. The fields and gradients imposed on the Polarized target will not be large but they must be compensated at the 10^{-4} level. Some magneto-static effort to model the target environment and design a compensation system is required.

2 Pre-Assembly and Fiducialization of the CPS

The CPS should be pre-assembled in the Test Lab. During assembly and after completion the CPS can be measured and fiducialized to facilitate final alignment in Hall C. Progressive measurement and fiducialization will eliminate problems with position references becoming hidden. Transporting the CPS to hall C in one piece will preserve the alignment and avoids introduction of errors due to dis-assembly and re-assembly. This would require a large crane in Hall C but no dis-assembly/re-assembly is required so it is likely to be the cheaper alternative. A comprehensive set of safety and operational test can be performed once CPS is assembled (see safety section following). to the movable platform (on the rollers) after experiment. Then the source will be stored in the hall until activation is sufficiently low for opening the shield.

3 Installation Considerations in Hall C

Installation of the CPS in Hall C will consist of the following steps:

- Removal of the Final Girder
- Remote girder dis-assembly and remount of instrumentation on the new girder
- Presurvey for mounting of the CPS stand.
- Mount CPS stand to Hall C floor

- 648 • Transport and Crane in complete CPS using a 150 Ton truck crane
- 649 • Survey and alignment of CPS
- 650 • Installation of new girder and instrumentation
- 651 • Survey and alignment of new girder
- 652 • Connect CPS magnet power and water and test
- 653 • Connect new girder and test
- 654 • Restore beam vacuum in Hall C

655 The CPS installation scheme is shown in Fig. 26.

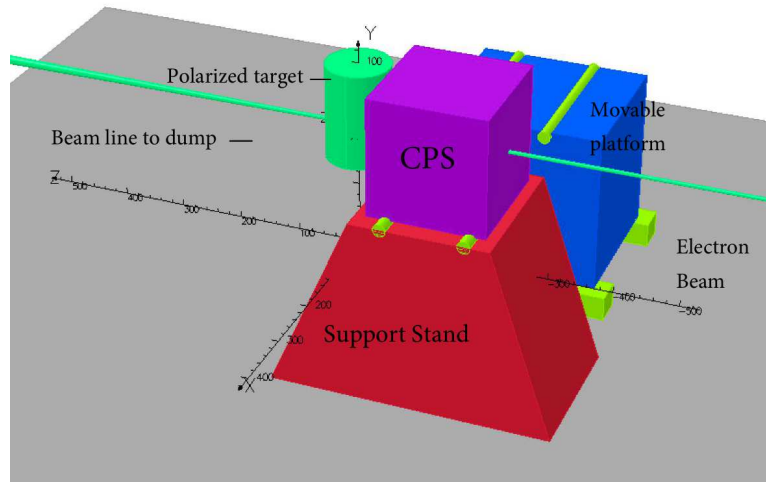


Figure 26. The CPS view in the hall. The electron beam is going from the right to the left. The movable platform (shown as a blue box) has two rails shown as green cylinders.

656 4 Interlocks, Instrumentation and Controls

657 The CPS should be heavily instrumented for early detection of problems such as low
 658 coolant flow, leaks, low pressure, high temperature, high conductivity etc. The protection
 659 and safety of the CPS begins with the design which must err on the side of conservatism
 660 especially in the magnet coil design and dump cooling. A very low current density design
 661 is suggested not to exceed 500 Amps/cm². Individual coil pancakes leads should be
 662 extended to an area outside of the magnet and shielding for easy access. There should
 663 be NO electrical or coolant joints inside the CPS shielding. Every separate sub coil of
 664 the CPS magnet should have thermometry, klixons and flow measurements to avoid any
 665 possibility that one of the separate current paths can overheat due to being starved of
 666 coolant, a leak or a bad electrical joint. Voltage monitoring of each sub coil is cheap
 667 insurance against overheating from any source including , internal blockage, leaks, flow

668 restrictions or bad electrical connections. Extra insulation between sub coils and between
669 the coil and ground can prevent ground faults. A commercial power supply is assumed and
670 these come with a wide array of internal interlock protections. The available interlocks
671 and signals would be fed into the FSD system to prevent damage.

672 5 Fast raster trip detection and raster interlocks

673 A dual protection scheme is suggested using both the Hall C BPM system and direct
674 instrumentation of the raster magnet itself. The BCMs would monitor beam position
675 and motion in close to real time and coil voltage monitoring on the raster coils would
676 provide ample early warning of raster problems. Both these independent signals would
677 be fed into the FSD system. Radiator temperature could be monitored to provide a
678 third independent protection system. Thermocouples mounted on the radiator should
679 be robust against radiation damage and should provide fast enough protection against
680 radiator overheating.

681 6 Safety Documentation and ERR process

682 The CPS will be required to have an ERR review since it represents a significant
683 new piece of experimental equipment for Hall C with new safety considerations. This
684 review process uses peer review with a combination of Lab and outside experts to study
685 the safety implications and review design and safety documents. This process has a set
686 of documentation requirements. The experiment itself will have its own set of standard
687 required documents. The CPS does not have any new safety considerations even though
688 it is a unique design. Hall C has had secondary in Hall water cooled dumps before of
689 comparable power. High power radiators are also not new. The combination of a high
690 power radiator, magnet and beam dump inside a shielded "box" imposes reliability and
691 remote handling considerations and these are the primary engineering controls providing
692 personnel protection. Satisfying the standard experiment documentation and ER process
693 should be completely adequate to insure overall safety of the CPS.

694 7 Commissioning plan for CPS and testing

695 A full pre-assembly and test of the CPS magnet, shielding cooling system and DC
696 power is suggested. The goals of this pre-assembly and test are to verify fit of all com-
697 ponents and to verify via life testing the magnet performance and cooling system. Sim-
698 ulations of various magnet failure modes such as reduced water flow, no water flow,
699 overheating etc. etc. can be used to proof test instrumentation. Interlocks and controls.
700 These tests would be repeated in Hall C after final installation and assembly.

701 8 Closed cycle CPS Cooling

702 Activation of the cooling water of the CPS magnet and beam dump is likely and a
703 closed cycle cooling system is suggested. The magnet heat and dump heat can be removed
704 thru a heat exchanger to either the Hall C air or LCW. Any activation of the CPS will be
705 confined to a very small volume and in the event of a leak external contamination will be
706 minimized. A leak pan under the CPS could easily be included to catch and confine any
707 leakage up to and including a total loss of primary coolant. A modular pallet mounted
708 design would be efficient and would include primary coolant pumps, DI resin beds, heat
709 exchanger, surge tank, controls, instrumentation and manifolds.

710 9 Post Experiment Removal Plan for CPS

711 The CPS is expected to become activated and contaminated by the completion
712 of the experiment. Exposure to Hall C staff will be minimized by designing the CPS
713 for a one-piece removal using a large truck crane. This eliminates the need for staff to
714 dis-assemble the CPS. Water disconnects using self-sealing connectors can be used to
715 eliminate any primary cooling water loss. The DC Power supply and air-cooled cables
716 will be disconnected and removed as they are not expected to be activated. The CPS will
717 be removed from hall C by truck to a safe storage location. The cooling water pumps,
718 controls, DI resin beds and heat exchanger will likely have contaminated water inside but
719 will not otherwise be activated. The cooling pallet can be removed to storage intact or
720 the water drained and stored separately or disposed of.

721 10 Cost Analysis

722 Preliminary cost analysis has be made by using vendor quotations for W-powder
723 and actual cost for the similar size normal conducting magnets.

- 724 • Tungsten powder shield, 64 tons, \$2400k
- 725 • The magnet yoke with permedur poles, 1.5 tons, \$10k + \$30k
- 726 • The coils with kapton tape isolation, \$30k
- 727 • Cu core absorber and closed loop water cooler, \$25k
- 728 • The WCu(20%) insert, 1 ton, \$100k
- 729 • Support structure and the elevation jacks, \$50k
- 730 • The beam line, radiator, and raster magnet with power supply, \$50k
- 731 • New Girder and rebuild estimate, 50K\$
- 732 • closed cycle magnet and dump cooling system, 25 K\$

- 733 • Instrumentation, controls, interlocks, PLC, 50K\$
- 734 • Rented crane and crew 5K\$/day (depends on crane size)

735 A total cost was found to be significant \$2.7M where the tungsten is a dominating
 736 part. Alternative shielding material is surplus lead which could be obtained (Oct. 2017)
 737 from SLAC for relatively low cost. However, it will increase the weight of the CPS from
 738 75 tons to 155 tons.

-
- 739 [1] D. Hamilton, “Photon Beam Requirements for Wide-Angle Compton Scattering”, in
 740 arXiv:1704.00816.
- 741 [2] D. Keller, “The UVa approved and proposed experiments”, in arXiv:1704.00816.
- 742 [3] B. Wojtsekhowski and G. Niculescu, “Conceptual Design Report, A Compact Photon
 743 Source”, Supplementary material for the WACS proposal PR12-15-003 to the JLab PAC
 744 43, June 2015; in arXiv:1704.00816.
- 745 [4] P.K. Kloeppel, “Design for 25-kW beam dumps at 100 MeV and 500 MeV”, CEBAF-TN-
 746 90-205; M. Wiseman, C.K. Sinclair, R. Whitney, M. Zarecky, “High Power Electron Beam
 747 Dumps at CEBAF”.

748 Appendix 1: Concept Transfer to Hall D

749 The intense photon source is one component of the K_L beam. The experimental
 750 method can be summarized as follows: electrons hit a copper radiator, the resulting
 751 photons hit a Be target, and a beam to K_L is produced. The search for missing hyperons
 752 is a strong motivation for this setup.

753 The new setup utilizes the Hall D Tagger vault, properly shielded by design to
 754 accomodate the medium power beam dump capable of accepting up to 60 kW of 12 GeV
 755 electron beam, assuming that proper local shielding is set around the dump. The presently
 756 installed dump is placed behind the iron labyrinth walls, and is surrounded by a massive
 757 iron shielding, made of iron blocks available at the time of construction. The standard
 758 GlueX setup is optimized for operations using very thin radiators producing relatively low
 759 intensity photon beam such that the beam electrons losing energy to photon production in
 760 the radiator may be detected and counted in the tagger hodoscope counters. The present
 761 setup is not suitable for production of massively more intense photon beams needed for
 762 the K_L production, due to the expected overwhelming radiation and activation levels in
 763 the vault.

765 The CPS will be located downstream of the tagger magnet. The tagger alcove has
 766 more space than that available in Hall A/C, so positioning and shielding placement are
 767 simpler. Indeed, the CPS implementation in Hall D may have a different length and
 768 magnet field, as well as shielding. A total floor loading of the implementation up to 100t
 769 is acceptable. If one uses a 2nd raster system for Hall D to compensate for the initial
 770 1mm raster, this can be an equivalent essential design to the Hall C/A one.

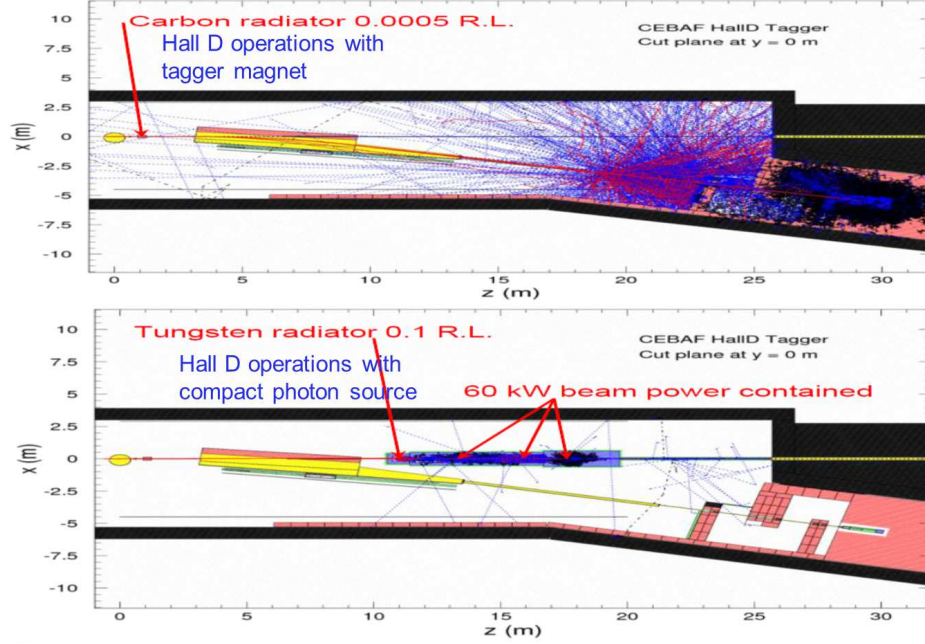


Figure 27. 2D projection of backgrounds in the Hall D alcove for both, the nominal GlueX beam/dump and the $5\mu\text{A}/\text{CPS}$ configuration.

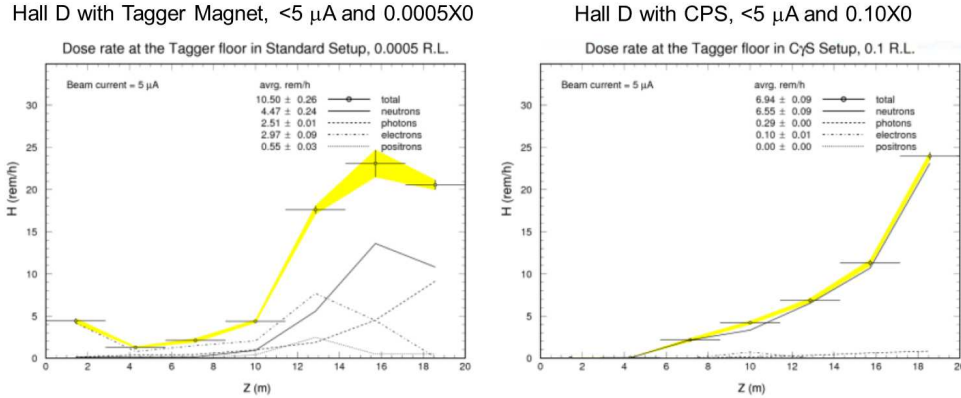


Figure 28. Dose rate at the tagger in standard configuration (left) and with CPS and 10% radiator (right). The CPS with its optimized shielding design does not increase radiation levels beyond standard configuration.

As discussed in section ??, the Compact Photon Source converts beam energies of up to 12 GeV with currents of up to $5\mu\text{A}$ into a high-intensity source of collimated photons. For the Hall-D adaptation, the $5\mu\text{A}$ beam current is limited by the design of the Hall D Tagger Magnet alcove. This corresponds to a 60 kW power limit. Note that the ceiling shielding of the Tagger hall above the CPS position is the same as it is above the existing 60 kW dump. No radiation increase at the site boundary is thus expected with respect to 60 kW operations using the existing dump. Figs. 27 and Fig. 28 illustrate how the CPS stops the electron beam and absorbs almost all beam energy inside, and therefore provides

779 excellent shielding. Running the CPS at full beam power produces radiation fields in the
780 Hall D tagger area, comparable with running regular Hall D experiment utilizing a very
781 thin radiator in front of the tagger magnet.

782 Appendix 2: Benchmark comparison

783 From the engineering standpoint, two of the most important aspects in the design
784 and subsequent building of a Compact Photon Source are the ability to properly shield the
785 radiation produced inside the source and to dissipate the resulting heat in a safe manner.
786 While the latter point was addressed earlier in this document, in this Appendix we focus
787 on the former issue, specifically detailing the steps taken to benchmark the simulations
788 used in assessing the prompt, as well as the residual (activation) radiation level around
789 the CPS and in the experimental Hall. Even though they have been mentioned before, it
790 is worth reiterating the basic radiation level constraints associated with experiments at
791 JLab:

792 From the radiological protection point of view the following set of limitations should
793 be satisfied, conservatively assuming typical expected experimental run conditions:

- 794 • Beam energy: 11.5 GeV Beam electron beam
- 795 • Current: $2.6 \mu A$
- 796 • Beam Power (based on the above) = 30 kW
- 797 • Run time: ~ 1000 hours

798 For the typical, high current JLab experiment the radiation dose rate parameters
799 must stay within the following limits:

- 800 • Dose rates in the Hall should be under several rem/h at 10 m from the device
- 801 • Dose rates at the boundary should be under $1 \mu rem/h$ during the run
- 802 • Dose rates outside the device envelope at a foot distance from the device should be
803 under several $mrem/h$ after one hour following the end of the 1000 hour run

804 In order to gain an understanding of the radiation levels likely to be produced by
805 the CPS and to ultimately design the optimal shielding for it, one relies on Monte Carlo
806 simulations and over the years the nuclear and particle physics community¹ has developed
807 a series of very sophisticated simulation programs. In time these programs became more
808 complex, with several physical processes that can be turned on and off, various thresholds
809 and cutoffs that might greatly influence the result yet they are buried deep inside the code.
810 Therefore, one has to be careful in using and interpreting the results of such simulations
811 because, as suggested above, the same simulation can give vastly (i.e. orders of magnitude
812 differences) different results with only (seemingly) minor changes in the input parameters.

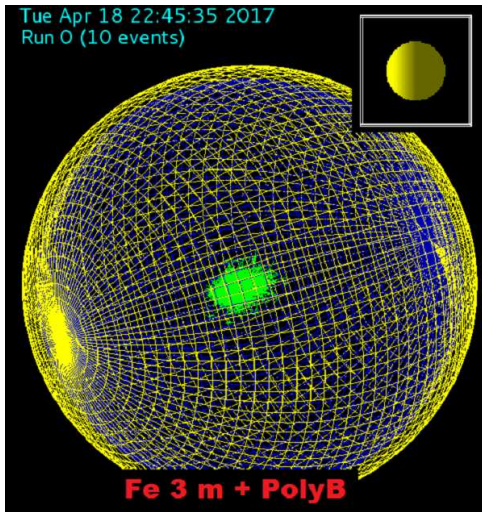
¹ As well as related areas such as nuclear medicine, astronomy, defense, etc.

813 Ideally one would want to **ground-truth** the simulation by **experimentally mea-**
 814 **suring** a small but relevant setup and verify that the simulation results agree with the
 815 measured radiation levels of that setup. For the current study this step was not done
 816 explicitly, though one can argue that one of the simulation programs used (Geant3) was
 817 extensively **ground-thruth-ed** as the JLab RadCon group compares the radiation levels
 818 measured at boundary of the experimental Halls with the Geant3 predictions.

819 To benchmark the simulations used in the CPS design a couple of relatively simple
 820 radiation scenarios were independently simulated using three different simulation pro-
 821 grams (Geant3², Fluka³, and Geant4⁴) by the three groups involved in this process, as
 822 follows:

- 823 • JLab group (led by P.D.): used Geant3
- 824 • UVa group (led by J.Z.): used Fluka
- 825 • JMU group (led by G.N.): used both Geant4 and Fluka

826 The geometry that was simulated was a simple sphere with a small cylindrical hole
 827 bored in it such that the 30 kW, 11.5 GeV beam interacts inside the sphere (at $z = 30$ cm
 828 for the Fe sphere and at $z = -15$ cm for the W sphere).



Four of these setups were simulated:

- A 300 cm diameter **Fe** sphere
- A 150 cm diameter **W** sphere
- A 300 cm diameter **Fe** sphere with an outer 10 cm Borated Polyethylene layer (5 % Boron by weight)
- A 150 cm diameter **W** sphere with an outer 10 cm Borated Poly layer

The results of these parallel simulations are summarized in the Table below.

Figure 29. Fe sphere with the Borated Poly layer, as simulated in Geant 4.

829
 830
 831 Examining these results one notes the reasonable agreement between the Geant3
 832 and Geant4 simulation, though factors of 1–2 could not be ruled out in the differences
 833 (and are to be expected in these types of estimations). The radiation levels predicted for
 834 these spheres leads one to conclude that the optimization of the CPS shielding satisfying
 835 the safety requirements in the Halls and outside ought to be possible. The addition of a
 836 borated polyethylene layer seems to be absolutely critical in moderating and absorbing

² The only code currently setup for calculating the radiation at the JLab boundary is Geant3.

³ Fluka is the only choice for activation calculations.

⁴ The development of the Fortran-based Geant3 code has ceased long time ago and the community has/is migrating toward the C++ based Geant4.

	Dose Rates [mrem/h]								
	JLab DINREG/Geant3			JMU Geant4			UVa Fluka		
	n	γ	total	n	γ	total	n	γ	total
3 m Fe	146	0.44	146.44	123.2	0.56	123.76	10	0.039	10.039
3 m Fe + Poly- B	0.8	2.8	3.6	0.284	0.56	0.844	0.11	0.063	0.173
1.5 m W	13	0.06	13.1	6.34	0.33	6.67	1.7	0.0002	1.7002
1.5 m W+Poly-B	2.7	0.003	2.7	1.76	1.28	3.04	0.15	0.0007	0.1507

Table I. Geant3, Fluka, and Geant4 prompt radiation comparison for Fe and W spheres.

low energy neutrons. This becomes very important if one chooses⁵ Fe as (part of) the shielding material.

One notes that a dose rate of $\sim 2.4 \mu\text{rem}/h$ at the boundary correspond to a "regular" normal experiment, not requiring extra shielding measures, corresponding to about the "200% of allowable design boundary dose rate" (that is, the dose rate at which the dose accumulation would be 10 mrem if such conditions are run for a half of the calendar year continuously).

The Fluka simulation (carried out in parallel at UVa and at JMU) was able to provide residual radiation (due to activation) at various time intervals: 1 hour, 24 hours, 7 days, 30 days. Sample results for the 3 m Fe sphere, one hour after the end of the irradiation cycle (assumed to be 1000 hours of 11.5 GeV, $2.6 \mu A$ beam) are shown in the Figures below.

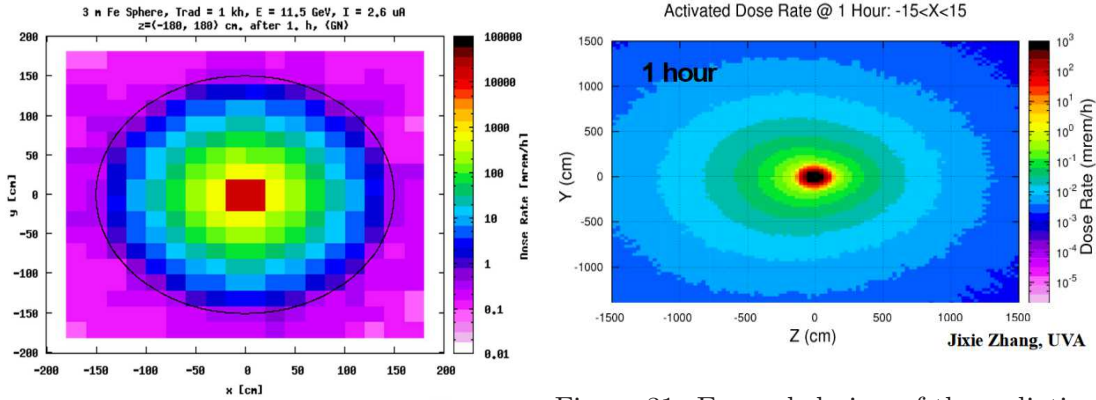


Figure 30. Radiation level one hour after the end of the irradiation period. Closeup view of the JMU Fluka result.

Figure 31. Expanded view of the radiation level one hour after the end of the irradiation period (UVa Fluka result). Both plots correspond to the 3 m Fe sphere.

⁵ For example for cost containment.